EPJ Applied Metamaterials manuscript No.
(will be inserted by the editor)

Fluorescence enhancement and strong-coupling in faceted plasmonic nanocavities

Nuttawut Kongsuwan [a,1], **Angela Demetriadou** [1,2], **Rohit Chikkaraddy** [3], **Jeremy J. Baumberg** [3], **Ortwin Hess** [b,1]

[1] Blackett Laboratory, Prince Consort Road, Imperial College London, London SW7 2AZ, UK
[2]School of Physics and Astronomy, University of Birmingham, Edgbaston, Birmingham B15 2TT, UK
[3]Cavendish Laboratory, University of Cambridge, Cambridge CB3 0HE, UK

Received: date / Accepted: date

Abstract Emission properties of a quantum emitter can be significantly modified inside nanometre-sized gaps between two plasmonic nanostructures. This forms a nanoscopic optical cavity which allows single-molecule detection and single-molecule strong-coupling at room temperature. However, plasmonic resonances of a plasmonic nanocavity are highly sensitive to the exact gap morphology. In this article, we shed light on the effect of gap morphology on the plasmonic resonances of a faceted nanoparticle-on-mirror (NPoM) nanocavity and their interaction with quantum emitters. We find that with increasing facet width the NPoM nanocavity provides weaker field enhancement and thus less coupling strength to a single quantum emitter since the effective mode volume increases with the facet width. However, if multiple emitters are present, a faceted NPoM nanocavity is capable of accommodating a larger number of emitters, and hence the overall coupling strength is larger due to the collective and coherent energy exchange from all the emitters. Our findings pave the way to more efficient designs of nanocavities for room-temperature light-matter strong-coupling, thus providing a big step forward to a non-cryogenic platform for quantum technologies.

Keywords Nanoplasmonics · Nanophotonics · Light-matter Strong-coupling · Fluorescence Enhancement · Quenching

1 Introduction

The decay lifetime of an excited quantum emitter is determined by both its intrinsic properties and its optical environment, as theoretically proposed by Purcell [1]. Since then, the effect has been verified experimentally on various optical-field enhancing environments [2–5]. One example of such an environment is a plasmonic nanostructure which has the ability to provide sub-wavelength light confinement and dramatically enhance the excitation and emission of an emitter [6]. However, placing an emitter too close to a single metal nanostructure quenches its far-field emission as the emitter dominantly decays into the non-radiative channels of the nanostructure [7, 8]. To suppress this quenching, the emitter can be placed inside a nanocavity formed by two closely spaced metallic nanostructures, i.e. a gap of few nanometres [9].

In our previous study, we experimentally and numerically demonstrated a suppression of fluorescence quenching for an emitter placed in a nanoparticle-on-mirror (NPoM) nanocavity [10]. In that study, we considered perfectly spherical nanoparticles (NPs). However, this does not always reflect experimental set-ups where NPs are in most cases faceted. Indeed, the spectral behavior of NPoM nanocavities also shows a highly sensitive relationship with its gap morphology. The facet widths of the NPoM nanocavities are hence also expected to greatly influence the field enhancement experienced by quantum emitters.

In this article, we use finite-difference time-domain (FDTD) method to investigate the effects of facet widths on the fluorescence enhancement, fluorescence quenching and strong-coupling of emitters in the NPoM nanocavity. We find that, by increasing the facet width, the NPoM nanocavity provides a weaker field enhancement and less coupling strength to a single emitter since the effective mode volume increases with the facet width. However, if multiple emitters are present, the faceted NPoM nanocavities are capable of accommo-

[a]e-mail: n.kongsuwan15@imperial.ac.uk
[b]e-mail: o.hess@imperial.ac.uk

dating more emitters, and hence the coupling strength is larger due to the collective and coherent energy exchange from all the emitters [11].

2 Fluorescence enhancement and quenching

Fluorescence emission of an emitter is a two-step process involving excitation and relaxation decay. When the excitation rate γ_{exc} of the emitter is much slower than its total decay rate γ_{tot}, the excited emitter decays to its ground state before the next excitation event. In this weak excitation regime, fluorescence emissions are limited by the excitation events, and therefore the fluorescence enhancement is given by [8]:

$$\gamma_{\text{em}} = \gamma_{\text{exc}}\,\eta\,, \tag{1}$$

where η is the emitter's quantum yield. For an emitter located at position $\mathbf{r}_0$ with transition dipole moment $\boldsymbol{\mu}$ and transition frequency ω_0, its excitation rate γ_{exc} is determined by the local electric field $\mathbf{E}(\mathbf{r}_0)$ in the direction of $\boldsymbol{\mu}$, $\gamma_{\text{exc}} \propto |\boldsymbol{\mu}\cdot\mathbf{E}(\mathbf{r}_0)|^2$. In vacuum, the emitter can only experience the incident field $\mathbf{E}_0(\mathbf{r}_0)$ whereas, in non-vacuum, the emitter experiences the local field $\mathbf{E}(\mathbf{r}_0)$ which is the combination of $\mathbf{E}_0(\mathbf{r}_0)$ and its secondary field reflected from the environment. Let us represent the excitation enhancement through the normalized rate:

$$\tilde{\gamma}_{\text{exc}} = \frac{\gamma_{\text{exc}}}{\gamma^0_{\text{exc}}} = \left|\frac{\hat{\boldsymbol{\mu}}\cdot\mathbf{E}(\mathbf{r}_0)}{\hat{\boldsymbol{\mu}}\cdot\mathbf{E}_0(\mathbf{r}_0)}\right|^2, \tag{2}$$

where γ^0_{exc} is the excitation rate of the emitter in vacuum and $\hat{\boldsymbol{\mu}}$ is a unit vector in direction of $\boldsymbol{\mu}$.

Each decay event either channels energy into a far-field radiation or is dissipated in the environment. The quantum yield $\eta = \gamma_{\text{rad}}/\gamma_{\text{tot}}$ provides a measure of this behavior and is defined as the ratio between far-field radiative decay rate γ_{rad} and the total decay rate γ_{tot} of the emitter. On the basis of Fermi's golden rule, γ_{tot} can be expressed in terms of the electromagnetic density of states $\rho(\mathbf{r}_0,\omega_0)$ as [12]:

$$\gamma_{\text{tot}} = \frac{2\omega_0}{3\hbar\epsilon_0}|\boldsymbol{\mu}^2|\rho(\mathbf{r}_0,\omega_0). \tag{3}$$

Assuming that the emitter does not have an intrinsic loss, its radiative decay rate $\gamma_{\text{rad}} = \gamma_{\text{tot}} - \gamma_{\text{nr}}$ can be indirectly found by calculating the non-radiative decay rate γ_{nr}. In the case of a plasmonic environment, γ_{nr} is predominantly determined by Ohmic losses [12]:

$$\gamma_{\text{nr}} \propto \int_V \text{Re}\left\{\mathbf{j}_{\text{ind}}(\mathbf{r})\cdot\mathbf{E}^*_{\text{em}}(\mathbf{r})\right\} d\mathbf{r}^3, \tag{4}$$

where $\mathbf{j}_{\text{ind}}$ is the induced current density within the volume V and $\mathbf{E}_{\text{em}}$ is the field emitted by the emitter. We define the radiative and non-radiative decay enhancements as the emitter's decay rates normalized to its decay rate in vacuum γ^0_{rad} as $\tilde{\gamma}_{\text{rad}} = \gamma_{\text{rad}}/\gamma^0_{\text{rad}}$ and $\tilde{\gamma}_{\text{nr}} = \gamma_{\text{nr}}/\gamma^0_{\text{rad}}$ respectively. The fluorescence enhancement is similarly defined as $\tilde{\gamma}_{\text{em}} = \tilde{\gamma}_{\text{exc}}\,\eta$.

A plasmonic nanostructure provides an ideal environment for fluorescence enhancement as it substantially amplifies both γ_{exc} and γ_{tot} of an emitter by confining light to a sub-wavelength volume and therefore substantially amplifying the electromagnetic density of states. However, the emitter in a plasmonic environment also experiences a large γ_{nr} due to Ohmic losses, which reduces η. Because of these competing factors, a specific plasmonic nanostructure can either potentially enhance or quench fluorescence.

3 Suppression of fluorescence quenching in faceted plasmonic nanocavities

Fluorescence quenching is observed when an emitter is placed too close to an isolated plasmonic nanostructure [7]. In the case of an isolated NP, for example, its optical response can be described as a multipole expansion of its surface plasmon (SP) modes [13]. The lowest-order dipole SP is the only mode that has a non-zero dipole moment and couples to the far-field radiation. On the other hand, the higher order modes confine light more strongly within a smaller volume surrounding the NP than the first order mode. As the emitter gets closer than 10 nm to the NP, it becomes dominantly coupled to the non-radiative higher-order modes of the NPs, and as a result, its fluorescence is quenched through energy dissipation in metal [8]. This is, however, not a general feature for all plasmonic nanostructures and in Ref. [10] we demonstrate the suppression of fluorescence quenching in a plasmonic nanocavity.

A plasmonic nanocavity emerges when two plasmonic nanostructures are brought together forming a gap of just a few nanometres. At such small gaps, the non-radiative SP modes of one nanostructure can couple with the radiative modes of the other nanostructure, and vice versa [13]. As a consequence, the hybridized higher-order modes of the combined structure gain radiative nature, and fluorescence quenching is hence suppressed in a plasmonic nanocavity. The hybridized SPs, called bonding SPs, also provide a massive field confinement inside the gap, allowing ultrasensitive detection down to single-emitter level [14,15]. Indeed, plasmonic structures have been developed for fluorescence enhancement and single-emitter detection, such as core-shell nanodumbbells [14], bowtie nanoantennas [16,17]

and film-coupled nanocubes [18]. In this article, we focus on the nanoparticle-on-mirror (NPoM) geometry, which is experimentally realized by assembling molecular layers in-between a spherical nanoparticle (NP) and a metal film (mirror) to form a nanocavity. The NPoM nanocavity has the advantage of providing sub-nanometre precision control over the spacing between a metallic NP and its mirror by using molecular layers, such as graphene [19], Cucurbituril [20] and DNA-origami [21].

3.1 Faceted NPoM nanocavities

So far we assumed that NPs are perfectly spherical. However, SEM images and experimental results [22,23] show that NPs are always faceted. Here, we investigate the fluorescence emission of an emitter inside a faceted NPoM nanocavity formed by a gold NP with diameter $2R = 80$ nm and facet widths $f = 0$, 5 and 10 nm atop a dielectric spacer with thickness $d = 5$ nm and a gold mirror, see Fig. 1(a). As we previously demonstrated [10], such a nanocavity can be fabricated using DNA origami (refractive index $n = 2.1$) to precisely control the positions of emitters in the nanocavity.

The bonding SPs of the NPoM nanocavity provide a large field enhancement $|\mathbf{E}|/|\mathbf{E}_0|$ in the gap region. The electric field distribution of the lowest-order bonding plasmon, the bonding dipole plasmon (BDP), is shown in Fig. 1(b) for an NPoM with $f = 10$ nm. The spectral positions of the BDPs for NPoM nanocavities with $f = 0$, 5 and 10 nm are summarized in Fig. 1(c) in the form of scattering cross-sections σ_{scat}. The dominant peaks σ_{scat} correspond to the BDPs, which redshift from 690 to 730 nm as facet widths increase. The peaks around 570 nm correspond to second-order bonding quadrupole plasmons (BQP), and they are spectrally less affected by the facet widths. For comparison, σ_{scat} for NPs placed on plain dielectric substrates are also shown in Fig. 1(c) and also exhibit first-order localized surface plasmons at ∼570 nm.

3.2 Suppression of fluorescence quenching

When a quantum emitter is placed in a NPoM nanocavity, the large field enhancement of the BDP massively enhances the excitation rate $\tilde{\gamma}_{\text{exc}}$. However, the fluorescence enhancement of the emitter also depends on the quantum yield η, and a large $\tilde{\gamma}_{\text{exc}}$ alone is not a sufficient condition for suppressing fluorescence quenching.

Here, we investigate the fluorescence emission in faceted NPoM nanocavities. Fig. 2 shows the rate enhancements $\tilde{\gamma}_{\text{rad}}$, $\tilde{\gamma}_{\text{nr}}$, $\tilde{\gamma}_{\text{exc}}$ and $\tilde{\gamma}_{\text{em}}$ computed by placing a classical dipole emitter at 2.5 nm below the NPs for faceted NPoM nanocavities and NPs on dielectric substrates. The results for each nanostructure are evaluated at the resonance frequency of the nanostructure's dominant plasmon modes, as shown in Fig. 1(c).

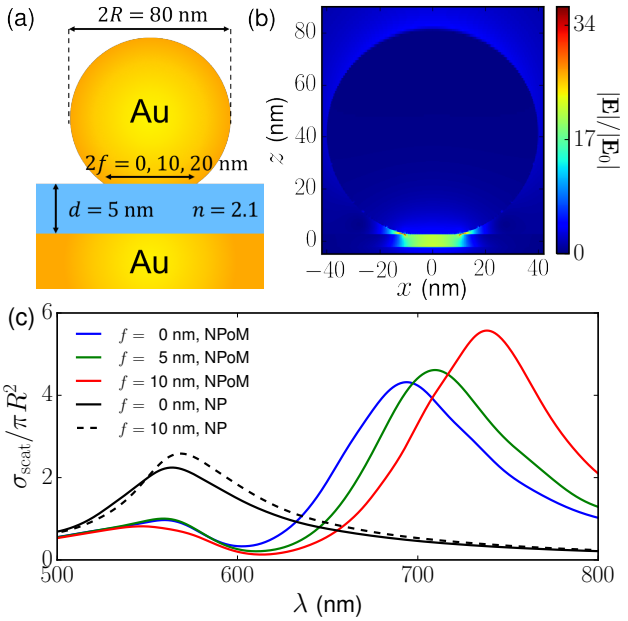


Fig. 1 (a) Schematic diagram of a nanoparticle-on-mirror (NPoM) nanocavity with diameter $2R = 80$ nm, facet diameter $2f$ and gap size $d = 5$ nm. (b) The field enhancement distribution $|\mathbf{E}|/|\mathbf{E}_0|$ of the bonding dipole plasmon (BDP) of the NPoM with $f = 10$ nm (c) Scattering cross-section σ_{scat} for the NPoM with $f = 0$, 5 and 10 nm and for nanoparticles (NPs) on plain dielectric substrates with $f = 0$ and 10 nm.

As the facet width increases, the NPs experience the lightning rod effect at their sharp facet edges, and consequently the rate enhancements of the emitters reach maxima near the facet edges, as seen in Fig. 2(b-e), dashed and dash-dotted lines. By contrast, the rate enhancements for the NPoM nanocavities are maximum at the center of the nanocavity for all facet widths. This is due to the nature of the BDPs which spatially confines the light field at the nanocavities' center. The NPoM nanocavities with larger facet widths also confine light less efficiently and possess larger effective mode volumes. Hence, the rate enhancements of the emitters spatially broaden with increasing facet width.

In the case of the NPs, its fluorescence $\tilde{\gamma}_{\text{em}}$ is quenched as $\tilde{\gamma}_{\text{nr}}$ dominates $\tilde{\gamma}_{\text{rad}}$ and gives a diminishing quantum yield $\eta < 0.03$ for both $f = 0$ and 10 nm. On the other hand, plasmon hybridization in the NPoM nanocavities provides sufficiently large $\tilde{\gamma}_{\text{rad}}$ and significant reductions in $\tilde{\gamma}_{\text{nr}}$, giving $\eta \approx 0.46$ at the center of the nanocavity for all facet widths. As shown in Fig. 2(e), the faceted NPoM nanocavities suppress fluores-

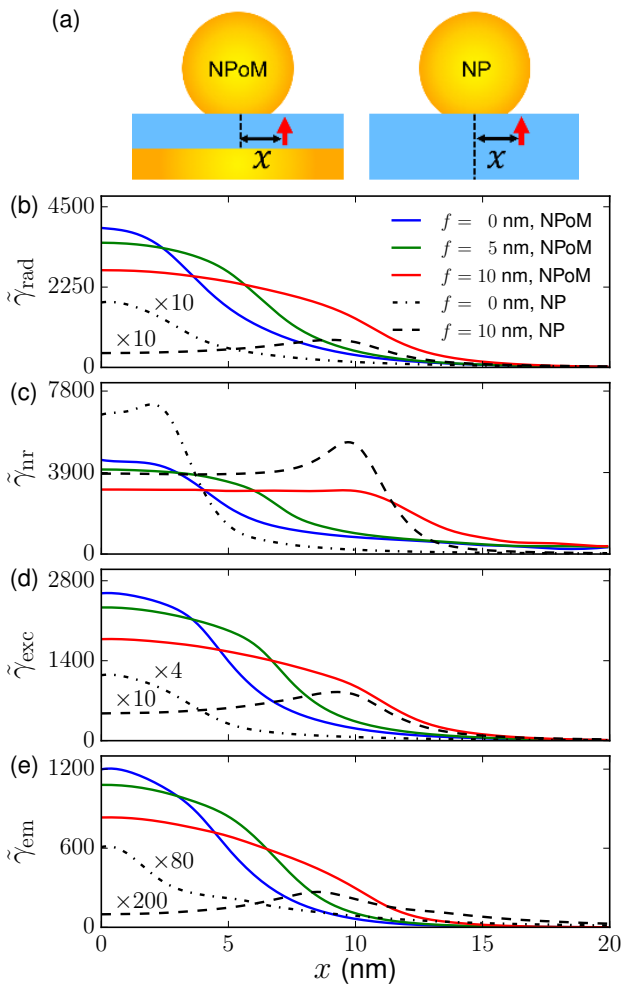


Fig. 2 (a) The radiative decay $\tilde{\gamma}_{\rm rad}$, (b) non-radiative decay $\tilde{\gamma}_{\rm nr}$, (c) excitation $\tilde{\gamma}_{\rm exc}$ and (d) fluorescence enhancements $\tilde{\gamma}_{\rm em}$ for the NPoM nanocavities with facet diameter $f = 0$, 5 and 10 nm and the NPs on dielectric substrates with $f = 0$ and 10 nm. For clarity, $\tilde{\gamma}_{\rm rad}$, $\tilde{\gamma}_{\rm exc}$ and $\tilde{\gamma}_{\rm em}$ for the NPs are multiplied by the indicated factors.

cence quenching of the emitters and provide more than two orders of magnitude increase in $\tilde{\gamma}_{\rm em}$, compared to the faceted NPs without the mirror. Hence, a faceted NPoM nanocavity with $f \leq 10$ nm retains the ability to suppress quenching. Unlike single NPs, the large η of NPoM nanocavities, with facet width $f < 10$ nm, allow information of the emitter-plasmon interaction to be observed by far-field detectors. Hence, the NPoM nanocavities, faceted or not, provides an ideal environment to observe strong-coupling.

4 Strong-coupling in faceted NPoM nanocavities

The emission properties of an emitter are influenced by its interaction with its optical environment. If the interaction is weak, only the emission rate is modified whereas the emission frequency remains unaltered. This is known as the weak-coupling regime. However, when the interaction is sufficiently strong, energy is reversibly exchanged between the two systems, and the electronic state of the emitter becomes inextricably mixed with the optical environment. In this strong-coupling regime, the resulting hybrid states split in energy and greatly differ from the original state of either constituent above.

To appreciate this process in the NPoM systems, let us consider an electronic (optical) state with resonance frequency ω_0 ($\omega_{\rm p}$) and spectral linewidth Γ_0 ($\Gamma_{\rm p}$). The hybrid state frequencies Ω_+ and Ω_- can be expressed as complex numbers of which the real parts ω_+ and ω_- correspond to their resonance frequencies and imaginary parts Γ_+ and Γ_- to their spectral linewidths [24]. At resonance, $\omega_0 = \omega_{\rm p}$, these are given by:

$$\Omega_\pm = \omega_0 - i\frac{1}{2}(\Gamma_{\rm p} + \Gamma_0) \pm \frac{1}{2}\sqrt{(2g)^2 - (\Gamma_{\rm p} - \Gamma_0)^2}, \quad (5)$$

where $g \propto \mu\sqrt{N/V}$ is the coupling strength which depends on the number N of emitters and the optical mode volume V [25]. The criteria for strong-coupling is when the energy splitting is larger than the new spectral width $\sqrt{(2g)^2 - (\Gamma_{\rm p} - \Gamma_0)^2} > \Gamma_{\rm p} + \Gamma_0$ which corresponds to $g > \sqrt{(\Gamma_{\rm p}^2 + \Gamma_0^2)/2}$.

In plasmonics, although metal nanostructures provide a large field confinement $1/V$ and coupling strength g, they suffer from rapid Ohmic dissipation which results in a large $\Gamma_{\rm p}$. Consequently, strong-coupling in plasmonics is often achieved through a coherent coupling with a collection of emitters. However, recent experiments by Chikkaraddy et al. [20] shows that certain NPoM nanocavities can provide such a massive field enhancement ($\sim 10^3$) to sufficiently compensate for its Ohmic dissipation and achieve single-molecule strong-coupling even at room temperature. Here, we focus on the far-field and near-field spectral responses of the emitter-plasmon strong-coupling in faceted NPoM nanocavities.

4.1 Far-field spectral response

Due to the nanoscale size of plasmonic structures, strong-coupling in this field is often observed via far-field measurements [20,26]. Therefore, we consider a collection of N emitters in the NPoM nanocavity. We place the emitters in a hexagonal lattice with lattice separation 2.5 nm. For $N = 1$, a single emitter is placed at the nanocavity's center. As more emitters are placed in the nanocavities, the emitters occupy the immediate neighboring sites outwards. The transitional frequency

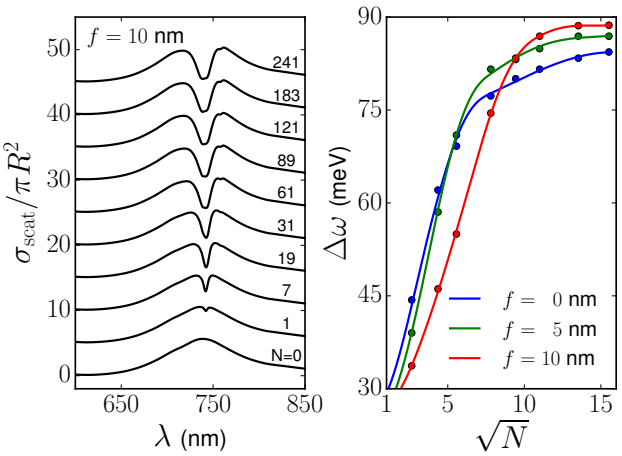


Fig. 3 (a) Scattering cross-sections $\sigma_{\rm scat}$ of the NPoM with $f = 10$ nm accommodating N quantum emitters as indicated. Each line is offset by $5\pi R^2$. (b) Spectral splitting $\Delta\omega = \omega_+ - \omega_-$ of the hybrid states between N emitters and BDPs of the NPoM with $f = 0$, 5 and 10 nm. The N emitters are organized in a hexagonal lattice with lattice spacing 2.5 nm.

for the emitters is set to the corresponding BDP mode for each facet width of NPoM.

The energy splitting due to the coupling between the BDP and N emitters can be observed as a peak splitting in the scattering cross-section $\sigma_{\rm scat}$, shown in Fig. 3(a) for an NPoM nanocavity with $f = 10$ nm. The corresponding energy splitting $\Delta\omega$ for facet widths $f =$ 0, 5 and 10 nm are also summarized in Fig. 3(b). For small emitter numbers $\sqrt{N} < 5$, the NPoM nanocavities with smaller facets provide stronger field enhancements and therefore exhibit larger $\Delta\omega$. As N increases, the energy splitting follows a linear relationship with $\sqrt{N}$, implying that all emitters coherently exchange energy with plasmons. On the other hand, for $\sqrt{N} > 10$, $\Delta\omega$ becomes saturated for all faceted NPoM nanocavities. The saturation points indicate the extent of the BDP mode volume beyond which further addition of emitters no longer changes the coupling strength. The NPoM nanocavities with larger facets provide larger mode volumes which can accommodate more emitters.

4.2 Near-field spectral response

The scattering cross-sections $\sigma_{\rm scat}$ provides partial information on the nanostructures' plasmonic response. These quantities only reflect the far-field collective behavior of all emitters inside and outside the NPoM nanocavities. In order to gain an insight into the individual coupling of each emitter, we investigate the near-field response.

The near-field optical responses of the NPoM nanocavity with N emitter are shown, in Fig. 4, as spatio-spectral field profile $|\mathbf{E}(x, \lambda)|$ evaluated at 1 nm above the mirror and along the x-direction, Fig. 2(a), of the nanocavity. For empty ($N = 0$) nanocavities, the $f = 10$ nm faceted nanocavity exhibits a red shift and lower spatial field confinement compared to $f = 0$ nm, in accordance with the earlier analyses in Fig. 1(c) and 3(b). When small numbers of emitters, $N = 19$, are placed at the center of the nanocavity, Fig. 4(b,e), the spectral distributions split and show the spatio-spectral field profile of the hybrid states. The field distributions also reveal the exact locations of the emitters as sharp, discrete peaks due to the emitters' abilities to absorb and store electromagnetic energy. As N increases from 19 to 183, the nanocavity with $f = 0$ nm does not show a significant change in its field distribution. By contrast, the $f = 10$ nm nanocavity shows a greater participation of emitters in the coupling. This confirms the analysis in the previous section in which the NPoM nanocavities with larger facets are capable of accommodating more emitters.

5 Conclusion

In conclusion, we numerically demonstrate how the gap morphology of a nanoparticle-on-mirror (NPoM) nanocavity affects its interaction with quantum emitters. By increasing the NP's facet width at its contact with the mirror, the field enhancement inside the nanocavity is weakened in exchange for a larger effective volume. The analysis shows that, in the weak coupling regime, a NPoM nanocavity retains its ability to suppress fluorescence quenching of an emitter for facet radius < 10 nm. In the strong-coupling regime, we show that a nanocavity with a smaller facet provides a larger field enhancement and couples more strongly with a small number of emitters placed at or close to the center of the nanocavity. On the other hand, a nanocavity with a larger facet can accommodate more emitters and couple more strongly with a large collection of emitters. We envisage numerous applications, including fast-emitting single-photon sources, nonlinear optics, quantum chemistry and quantum technologies.

Acknowledgements We acknowledge support from EPSRC grants EP/G060649/1 and EP/L027151/1 and European Research Council grant LINASS 320503.

References

1. E. Purcell, Phys. Rev. 69 (1946) 681.

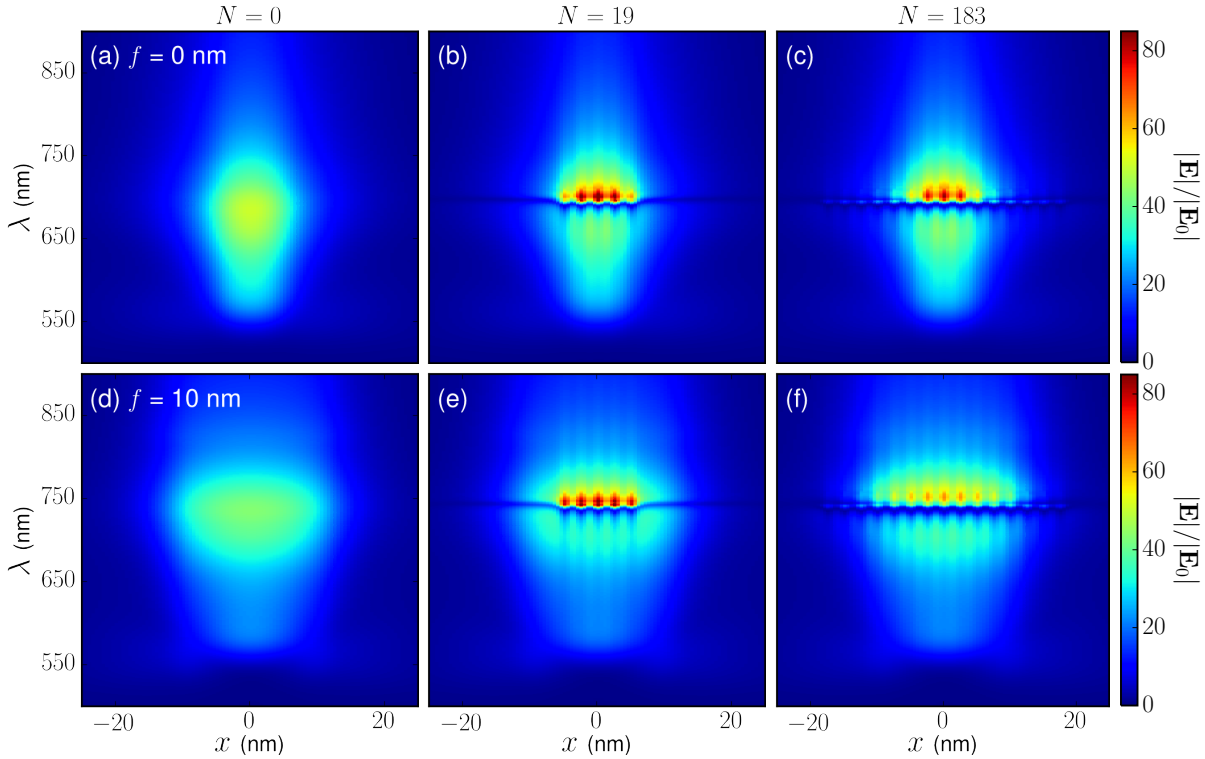


Fig. 4 Spatio-spectral field distributions $|\mathbf{E}(x,\lambda)|$ of the emitter-plasmon hybrid states for (a,d) $N = 0$, (b,e) $N = 19$, (c,f) $N = 183$ quantum emitters and (a,b,c) $f = 0$ nm and (d,e,f) $f = 10$ nm. The field distributions are evaluated at 1 nm above the mirror.

2. P. Goy, J.M. Haimond, M. Gross, S. Haroche, Phys. Rev. Lett. 50 (1983) 1903.
3. K. Drexhage, Prog. Opt. 12 (1974) 163-232.
4. D. Kleppner, Phys. Rev. Lett. 47 (1981) 233.
5. P. Lodahl, A.F. van Driel, I.S. Nikolaeva, A. Irman, K. Overgaag, D. Vanmaekelbergh, W.L. Vos, Nature 430 (2004) 654-657.
6. S. Kuhn, U. Hakanson, L. Rogobete, V. Sandoghdar, Phys. Rev. Lett. 97 (2006) 017402.
7. E. Dulkeith, A.C. Morteani, T. Niedereichholz, T.A. Klar, J. Feldmann, S.A. Levi, F.C.J.M. van Veggel, D.N. Reinhoudt, M. Moller, D.I. Gittins, Phys. Rev. Lett. 89 (2002) 203002.
8. P. Anger, P. Bharadwaj, L. Novotny, Phys. Rev. Lett. 96 (2006) 113002.
9. R. Faggiani, J. Yang, P. Lalanne, ACS Photonics 2 (2015) 1739-1744.
10. N. Kongsuwan, A. Demetriadou, R. Chikkaraddy, F. Benz, V.A. Turek, U.F. Keyser, J.J. Baumberg, O. Hess, ACS Photonics 5 (2017) 186-191.
11. A. Delga, J. Feist, J. Bravo-Abad, F.J. Garcia-Vidal, Phys. Rev. Lett. 112 (2014) 253601.
12. L. Novotny, B. Hecht, Principles of Nano-Optics, 2nd edn. (Cambridge University Press, Cambridge, 2012).
13. G. Sun, J. Khurgin, Appl. Phys. Lett. 97 (2010) 263110.
14. D.K. Lim, K.S. Jeon, H.M. Kim, J.M. Nam, Y.D. Suh, Nat. Mater. 9 (2010) 60-67.
15. H. Lee, J.H. Lee, S.M. Jin, Y.D. Suh, J.M. Nam, Nano Lett. 13 (2013) 6113-6121.
16. A. Kinkhabwala, Z. Yu, S. Fan, Y. Avlasevich, K. Mullen, W.E. Moerner, Nat. Photonics 3 (2009) 654-657.
17. K. Santhosh, O. Bitton, L. Chuntonov, G. Haran, Nature Communications 7 (2016) 11823.
18. G.M. Akselrod, C. Argyropoulos, T.B. Hoang, C. Ciraci, C. Fang, J. Huang, D.R. Smith, M.H. Mikkelsen, Nat. Photonics 8 (2014) 835-840.
19. J. Mertens, A.L. Eiden, D.O. Sigle, F. Huang, A. Lombardo, Z. Sun, R.S. Sundaram, A. Colli, C. Tserkezis, J. Aizpurua, S. Milana, A.C. Ferrari, , J.J. Baumberg, Nano Lett. 13 (2013) 5033-5038.
20. R. Chikkaraddy, B. de Nijs, F. Benz, S.J. Barrow, O.A. Scherman, E. Rosta, A. Demetriadou, P. Fox, O. Hess, J.J. Baumberg, Nature 535 (2016) 127-130.
21. R. Chikkaraddy, V. Turek, N. Kongsuwan, F. Benz, C. Carnegie, T. Van De Goor, B. de Nijs, A. Demetriadou, O. Hess, U.F. Keyser, J.J. Baumberg, Nano Lett. 18 (2017) 405-411.
22. D.O. Sigle, J. Mertens, L.O. Herrmann, R.W. Bowman, S. Ithurria, B. Dubertret, Y. Shi, H.Y. Yang, C. Tserkezis, J. Aizpurua, J.J. Baumberg, ACS Nano 9 (2015) 825-830.
23. J. Mertens, A. Demetriadou, R.W. Bowman, F. Benz, M.E. Kleemann, C. Tserkezis, Y. Shi, H.Y. Yang, O. Hess, J. Aizpurua, J.J. Baumberg, Nano Lett. 16 (2016) 5605-5611.
24. P. Torma, W.L. Barnes, Rep. Prog. Phys. 78 (2015) 013901.
25. C. Sauvan, J.P. Hugonin, I. Maksymov, P. Lalanne, Phys. Rev. Lett. 110 (2013) 237401.
26. R.W. Boyd, Non-linear Optics (Elsevier, United States of America, 2008).
27. S. Wuestner, A. Pusch, K.L. Tsakmakidis, J.M. Hamm, O. Hess, Philos. Trans. R. Soc., A 369 (2011) 3525-3550.

Appendix A: Maxwell-Bloch description

In Sec. 2 and 3, a classical dipole emitter is used to study the Purcell enhancement effect in the weak-coupling regime. This classical model is not sufficient to study the light-matter strong-coupling dynamics as we require a model which simultaneously describes the excitation of plasmons and their coupling to emitters. In Sec. 4, the emitters are considered semi-classically using two-level Maxwell-Bloch description with Hamiltonian [26]:

$$\hat{H} = \hat{H}_0 + \hat{V}(t) = \hbar\omega_0\hat{\sigma}^\dagger\hat{\sigma} - \hat{\boldsymbol{\mu}}\cdot\mathbf{E},$$

where $\hat{\sigma}$ denotes the exciton annihilation operator, $\hat{\boldsymbol{\mu}} = \boldsymbol{\mu}(\hat{\sigma}^\dagger + \hat{\sigma})$ is the transitional dipole moment operator and ω_0 the transition frequency. The emitter is modeled after the Cy5 molecule with $\mu = 10.1$ D. We can treat the system of an emitter inside a NPoM nanocavity as an open quantum system and express the problem using the density matrix $\hat{\rho}$ approach and Lindblad master equation:

$$\frac{\partial\hat{\rho}}{\partial t} = \frac{-i}{\hbar}\left[\hat{H},\hat{\rho}\right] + \frac{\gamma_r}{2}(2\hat{\sigma}\hat{\rho}\hat{\sigma}^\dagger - \hat{\sigma}^\dagger\hat{\sigma}\hat{\rho} - \hat{\rho}\hat{\sigma}^\dagger\hat{\sigma}) + \frac{\gamma_p}{2}(2\hat{\sigma}^\dagger\hat{\rho}\hat{\sigma} - \hat{\sigma}\hat{\sigma}^\dagger\hat{\rho} - \hat{\rho}\hat{\sigma}\hat{\sigma}^\dagger) + \frac{\gamma_d}{2}(\hat{\sigma}_z\hat{\rho}\hat{\sigma}_z - \hat{\rho}),$$

where $\hat{\sigma}_z = \hat{\sigma}^\dagger\hat{\sigma} - \hat{\sigma}\hat{\sigma}^\dagger$ and γ_r, γ_p and γ_d denote incoherent relaxation rate, incoherent pumping rate and pure dephasing rate respectively. Solving the above equation, we obtain:

$$\frac{\partial\rho_{22}}{\partial t} = -\frac{\partial\rho_{11}}{\partial t} = -\gamma[\rho_{22} - \rho_{22}^{SS}] - \frac{2}{\hbar}\boldsymbol{\mu}\cdot\mathbf{E}\ \mathrm{Im}(\rho_{12}),$$

$$\frac{\partial\rho_{12}}{\partial t} = \frac{\partial\rho_{21}^*}{\partial t} = -(\Gamma_0 - i\omega_0)\rho_{12} + \frac{i}{\hbar}\boldsymbol{\mu}\cdot\mathbf{E}(2\rho_{22} - 1),$$

where we define the total relaxation rate $\gamma = \gamma_r + \gamma_p = 0.66\ \mu$eV and the total dephasing rate $\Gamma_0 = \gamma_d + \gamma/2 = 3.98$ meV. The steady-state excited state population $\rho_{22}^{SS} = \gamma_p/(\gamma_r + \gamma_p)$ is negligible in our system where $\gamma_p \ll \gamma_r$ at an optical frequency and room temperature.

In our FDTD calculations, the simulation space is divided into a grid, and the plasmons (E-field) in each grid cell is obtained by solving the Maxwell equations. The emitters are driven by the plasmons and inject photons back to the simulation through a macroscopic polarization $\mathbf{P} = N_\mathrm{d}\,\mathrm{Tr}(\hat{\rho}\hat{\boldsymbol{\mu}}) = 2N_\mathrm{d}\,\hat{\boldsymbol{\mu}}\,\mathrm{Re}(\rho_{12})$, where N_d is the total carrier density. The dynamic equations for ρ_{ij} can then be expressed in terms of the polarization $\mathbf{P}$, ground state population $N_1 = N_\mathrm{d}\,\rho_{11}$ and excited state population $N_2 = N_\mathrm{d}\,\rho_{22}$ [27]:

$$\frac{\partial^2\mathbf{P}}{\partial t^2} + 2\Gamma_0\frac{\partial\mathbf{P}}{\partial t} + (\Gamma_0^2 + \omega_0^2)\mathbf{P} = -\frac{2\omega_0}{\hbar}\mu^2(N_2 - N_1)\mathbf{E}(t)$$

$$\frac{\partial N_2}{\partial t} = -\frac{\partial N_1}{\partial t} = -\gamma N_2 + \frac{1}{\hbar\omega_0}\left(\frac{\partial\mathbf{P}}{\partial t} + \Gamma_0\mathbf{P}\right)\cdot\mathbf{E}(t).$$